

Unusual Solvent Effect on a S_N2 Reaction. A Quantum-Mechanical and Kinetic Study of the Menshutkin Reaction between 2-Amino-1-methylbenzimidazole and Iodomethane in the Gas Phase and in Acetonitrile

André Melo,^{*,†} António J. I. Alfaia,[‡] João Carlos R. Reis,[§] and António R. T. Calado[‡]

REQUIMTE/Departamento de Química, Faculdade de Ciências, Universidade do Porto, Rua do Campo Alegre, 687, 4169-007 Porto, Portugal, Centro de Estudos de Ciências Farmacêuticas, Faculdade de Farmácia, Universidade de Lisboa, Av. Prof. Gama Pinto, 1649-003 Lisboa, Portugal, and Departamento de Química e Bioquímica, Centro de Electroquímica e Cinética, Faculdade de Ciências, Universidade de Lisboa, 1749-016 Lisboa, Portugal

Received: October 4, 2005; In Final Form: November 30, 2005

The quaternization reaction between 2-amino-1-methylbenzimidazole and iodomethane was investigated in the gas phase and in liquid acetonitrile. Both experimental and theoretical techniques were used in this study. In the experimental part of this work, accurate second-order rate constants were obtained for this reaction in acetonitrile from conductivity data in the 293–323 K temperature range and at ambient pressure. From two different empirical equations describing the effect of temperature on reaction rates, thermodynamic functions of activation were calculated. In the theoretical part of this work, the mechanism of this reaction was investigated in the gas phase and in acetonitrile. Two different quantum levels (B3LYP/[6-311++G(3df,3pd)/LanL2DZ]//B3LYP/[6-31G(d)/LanL2DZ] and B3LYP/[6-311++G(3df,3pd)/LanL2DZ]//B3LYP/[6-31+G(d)/LanL2DZ]) were used in the calculations, and the acetonitrile environment was modeled using the polarized continuum model (PCM). In addition, an atoms in molecules (AIM) analysis was made aiming to characterize possible hydrogen bonding. The results obtained by both techniques are in excellent agreement and lead to new insight into the mechanism of the reaction under examination. These include the identification and thermodynamic characterization of the relevant stationary species, the rationalization of the mechanistic role played by the solvent and the amine group adjacent to the nucleophile nitrogen atom, the proposal of alternative paths on the modeled potential energy surfaces, and the origin of the marked non-Arrhenius behavior of the kinetic data in solvent acetonitrile. In particular, the AIM analysis confirmed the operation of intermolecular hydrogen bonds between reactants and between products, both in the gas phase and in solution. It is also concluded that the unusual solvent effect on this Menshutkin reaction stems from the conjunction of a nucleophile possessing a relatively complex chemical structure with a dipolar aprotic solvent that is protophobic.

Introduction

Bimolecular nucleophilic substitution (S_N2) reactions are of great importance for both chemical and biochemical processes. These reactions are very common and occur in different environments, such as the gas phase,^{1–15} liquid solution,^{1,3,13,14,16–32} enzymes,^{33–36} zeolites,³⁷ and micelles.^{38,39} The thermodynamics and kinetics of these reactions have been studied extensively by different experimental techniques, for example, mass spectrometry,^{6,7,15,20,40} UV–visible spectrophotometry,^{16,17,24,25,29,38,39} conductivity,^{18,20,22,28,30} potentiometry,^{24,31} and NMR spectroscopy.²⁶

A significant amount of theoretical work has also been published on this subject. The mechanism of these reactions is usually studied by two main theoretical approaches: (a) identification and thermodynamic characterization of all stationary species occurring on the respective Born–Oppenheimer potential energy surface at appropriate quantum^{1–8,12–15,19,23,32,37,40,41} or hybrid quantum mechanics/molecular mechanics (QM/

MM)^{33,36} levels and (b) molecular simulations using classical,⁹ *ab initio*,^{10,11} or hybrid (QM/MM)^{3,21,27,34,35} potentials.

Many S_N2 reactions occurring in solution have been studied by theoretical methods, and three alternative models are usually used to model the solvent effect: (i) the supermolecule model that treats the solute and a small number of representative solvent molecules at the same quantum level,^{40,41} (ii) the hybrid model that describes the solute and eventually the first-solvation-shells solvent molecules by quantum methods and all of the other solvent molecules by molecular mechanics,^{3,21,27} and (iii) the continuum solvation method that represents the solvated system as a solute (super)molecule inserted in a cavity surrounded by a continuum environment characterized by a dielectric constant, ϵ .^{1,3,13,14,19,23,32}

In general, a S_N2 reaction can be represented by the following chemical equation,



where X is the nucleophile and Y is the leaving group. The schematic potential energy profiles for two hypothetical S_N2 reactions both in the gas phase and in solution are presented in Figure 1.

* Corresponding author. E-mail: asmelo@fc.up.pt.

[†] Faculdade de Ciências, Universidade do Porto.

[‡] Faculdade de Farmácia, Universidade de Lisboa.

[§] Faculdade de Ciências, Universidade de Lisboa.

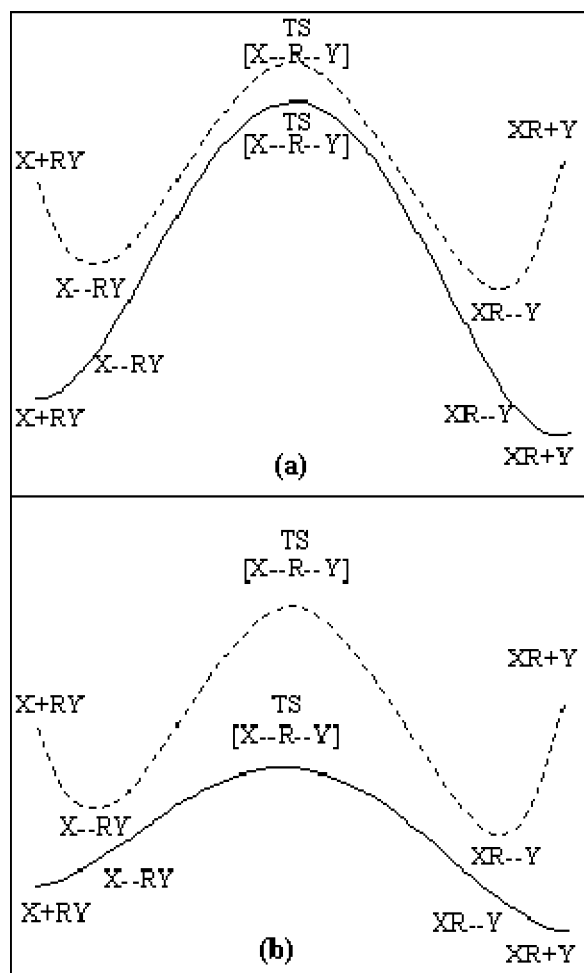


Figure 1. Schematic representation of potential energy surfaces in the gas phase (dashed line) and in solution (solid line) for (a) a S_N2 reaction with a transition state less polar than the separated reactants and (b) a S_N2 reaction with a transition state more polar than the separated reactants. All of the stationary species are identified ($X + RY$ = separated reactants, $X-RY$ = reactant binding complex, $[X-R-Y]$ = transition state, $XR-Y$ = product binding complex, $XR + Y$ = separated products). All of the mentioned species can be neutral or charged.

The transition state $[X-R-Y]$ usually has a trigonal bipyramidal geometry and is connected via the reaction coordinate with the binding complexes ($X-RY$ and $XR-Y$). In the gas phase, these complexes are usually more stable than the separated species ($X + RY$ and $XR + Y$), and this originates a double-well energy profile.^{3,12–14,27,32,41} In solution, because the separated species are usually more stabilized than the binding complexes (they have larger solvent-accessible areas) the energy adopts a unimodal profile.^{3,12–14,27,32,41} However, the solvent usually increases the activation energy for S_N2 reactions with a transition state less polar than the separated reactants^{3,12,13,41} and decreases this energy in the opposite case.^{14,27,32,42}

In this work, the quaternization reaction between 2-amino-1-methylbenzimidazole (AMBI) and iodomethane (MeI) (see Figure 2) is analyzed using experimental and theoretical approaches. The atoms of all of the species involved in the mechanism proposed for this reaction (including binding complexes and the transition state) are labeled according to the notation presented in Figure 2. AMBI is a 20-atom-strong organic molecule possessing 3 nitrogen atoms. The anticipated high degree of complexity for the quantum-mechanical description of a Menshutkin reaction involving such a nucleophile is,

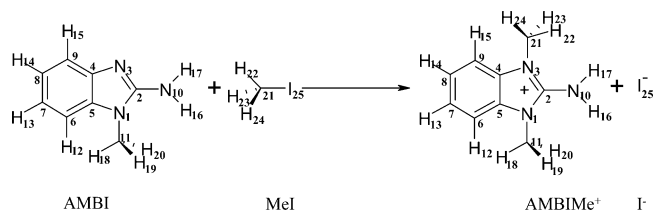


Figure 2. Chemical equation describing the quaternization reaction between 2-amino-1-methylbenzimidazole (AMBI) and iodomethane (MeI). A general notation to label the atoms of all of the species involved in the mechanism proposed for this reaction is presented.

however, counterbalanced by the essentially rigid and flat structure of this aromatic heterocyclic imine.

The results obtained by both experimental and theoretical approaches are in excellent agreement and allow us to propose a mechanism for this reaction in which the roles of the solvent and the N_{10} -amine group adjacent to the nucleophilic nitrogen (N_3) (see Figure 2) are of particular importance. Indeed, quantum-mechanical calculations revealed the formation of unusual binding complexes during the course of this Menshutkin reaction in acetonitrile. With this information at hand, we explain the experimentally observed non-Arrhenius temperature dependence of rate constants.

Methods

Experimental. Materials. MeI ($\geq 99.5\%$) was obtained from Fluka. AMBI (95%) from Aldrich was recrystallized twice from ethanol/propan-2-ol and dried in a desiccator over phosphorus pentoxide. Acetonitrile were purchased from Riedel de Haën ($\geq 99.9\%$). Spectrophotometric analysis confirmed that the solvent contained no organic impurities and the water content was kept lower than 0.02%. 2-Amino-1,3-dimethylbenzimidazolium iodide was prepared as described elsewhere.³⁰

Apparatus. A Wayne Kerr B905 bridge (accuracy $\pm 0.05\%$) and commercial conductivity cells (980-K19/120) were used to obtain the conductivity data from which rate constants and calibration curves were calculated. Cell constants ranged from 0.9 to 1.1 cm^{-1} . The kinetic experiments were carried out in a thermostated bath as described previously.^{43,44} The temperature was kept constant to within $\pm 0.01\text{K}$.

Kinetic Measurements. All solutions were prepared by weight in acetonitrile dried with oxygen-free nitrogen. Reacting solutions with equal initial concentrations in both reactants (between 0.01 and 0.02 mol dm^{-3}) were followed conductometrically up to 15–20% conversion. In this way, the disturbing effects from solvolysis and reverse Menshutkin reactions could be avoided in the rate measurements of the present reaction. For each kinetic run, a minimum of 150 data points were recorded. Triplicate kinetic runs were made at each temperature. By using a calibration procedure described elsewhere,^{30,43,44} conductivity data were converted into quaternary-salt concentrations. In this work, duplicate measurements for 10 calibrating solutions of 2-amino-1,3-dimethylbenzimidazolium iodide in the 0.0001–0.0075 mol dm^{-3} concentration range were made for each experimental temperature. Rate constants were then calculated from the slope of linear plots describing the integrated second-order rate law for equal initial concentration in both reactants, which gave excellent correlation coefficients. TLC analyses of the reaction mixtures, at the beginning and at the end of the kinetic experiments, were run on silica gel plates.

Computational. Four potential energy surfaces for the reaction under study were analyzed, modeling the gas phase and acetonitrile environments at two different lower quantum

levels (low). All of the stationary species identified on these surfaces were fully optimized, including the characterization of two isomeric forms and the calculation of the corresponding harmonic frequencies. A scaling factor of 0.9804 was used to correct for the well-known systematic error in the vibrational zero point and thermal Gibbs energy.⁴⁵ Transition states were characterized by a single imaginary frequency, which is associated with the reaction coordinate describing the motion of the C₂₁-methyl group between the iodine atom (I₂₅) and the nucleophilic nitrogen atom (N₃). For each identified transition state, an intrinsic reaction coordinate (IRC) analysis⁴⁶ was carried out to ensure that it is connected via reaction coordinate with the appropriate usual binding complexes. For each potential energy surface, two conformational analyses were performed to study (hydrogen-bonded binding complex)–(usual binding complex) interconversion processes in both sides of the potential energy barrier. The (N₃–C₂₁–I₂₅) bond angle was selected as an appropriate conformational coordinate for these analyses. Single-point corrections (corr) were calculated for all of the mentioned stationary species at a higher quantum level. Standard states with concentrations of 1 mol dm^{−3} at 298.15 K were adopted for all of the calculations. An ambient pressure of 1 atm was considered for the acetonitrile environment.

All of the calculations were performed with the hybrid density functional B3LYP method,^{47–50} and the LanL2DZ basis set⁵¹ was always used for iodine. The other atoms were described by the 6-31G(d) and 6-31+G(d) basis sets for the calculations carried out at the two alternative lower quantum levels and by the very accurate 6-311++G(3df,3pd) basis set for the single-point corrections carried out at the higher quantum level. The two different combined (corr + low) quantum levels used in this work will be referred to as B3LYP/[6-311++G-(3df,3pd)/LanL2DZ]/B3LYP/[6-31G(d)/LanL2DZ] and B3LYP/[6-311++G(3df,3pd)/LanL2DZ]/B3LYP/[6-31+G(d)/LanL2DZ]. The acetonitrile environment was modeled by the polarizable continuum model (PCM),⁵² which has been demonstrated to be appropriated to reproduce the effect of aprotic solvents such as acetonitrile.⁵³ An additional atoms in molecules (AIM) analysis^{54,55} was also carried out for each structure where the existence of hydrogen bonds is expected. All of the calculations have been performed with the GAUSSIAN03⁵⁶ package on a Pentium 4 computer. The AIM analysis has been carried using the AIMPAC series of programs.⁵⁷

According to the PCM formalism,⁵² the Gibbs energy ($G^{(sol)}$) of a given species, X, in solution can be calculated as

$$G^{(sol)} = G_{sp}^{(sol)} + G_{mol.mot.}^{(sol)} + (PV)^{(sol)} \quad (2)$$

where $G_{sp}^{(sol)}$ is the Gibbs energy of solvated solute X at a fixed geometry (single-point Gibbs energy), $G_{mol.mot.}^{(sol)}$ is the Gibbs energy associated with molecular motions (translations, rotations, and vibrations), and $(PV)^{(sol)}$ is the enthalpic correction (P being the pressure and V the volume) associated with the adopted standard state.

The single-point Gibbs energy can be decomposed into two components:

$$G_{sp}^{(sol)} = G_{el}^{(sol)} + G_{solvent}^{(sol)} \quad (3)$$

In eq 3, $G_{el}^{(sol)}$ is the total electronic energy of solute X, which is calculated taking into account the polarization effects of the reaction field induced by the continuum dielectric environment. This component is given by the sum of its electronic ($E_{el}^{(sol)}$) and nuclear repulsion ($E_{NR}^{(sol)}$) energies:

$$G_{el}^{(sol)} = E_{el}^{(sol)} + E_{NR}^{(sol)} \quad (4)$$

In the former equation, $G_{solvent}^{(sol)}$ is the component associated with the solvent, which includes terms for solvent rearrangement (polarization ($G_{pol}^{(sol)}$) and cavitation ($G_{cav}^{(sol)}$)) and for solute–solvent (electrostatic ($G_{es}^{(sol)}$) and nonelectrostatic ($G_{n/es}^{(sol)}$)) interactions. Thus

$$G_{solvent}^{(sol)} = G_{pol}^{(sol)} + G_{cav}^{(sol)} + G_{es}^{(sol)} + G_{n/es}^{(sol)} \quad (5)$$

In the gas phase, the component associated with the solvent does not operate and the equation for the Gibbs energy of species X can be expressed as

$$G^{(g)} = G_{sp}^{(g)} + G_{mol.mot.}^{(g)} + (PV)^{(g)} = G_{el}^{(g)} + G_{mol.mot.}^{(g)} + (PV)^{(g)} = E_{el}^{(g)} + E_{NR}^{(g)} + G_{mol.mot.}^{(g)} + (PV)^{(g)} \quad (6)$$

Every component in eq 6 has the same physical meaning as discussed below for the corresponding component in the case of reactions in solution but for the fact that they are associated with species X in a vacuum environment.

According to the methodology adopted in this work, the single-point Gibbs energy of each species X in a given environment (env = sol or g) is calculated, except for the contribution from nuclear repulsion, as a sum of two terms, one calculated at a lower (low) level and the other at a higher (corr) level

$$G_{sp}^{(env)} = G_{sp,low}^{(env)} + G_{sp,corr}^{(env)} \quad (7)$$

$$G_{el}^{(env)} = G_{el,low}^{(env)} + G_{el,corr}^{(env)} \quad (8)$$

$$G_{solvent}^{(env)} = G_{solvent,low}^{(env)} + G_{solvent,corr}^{(env)} \quad (9)$$

$$E_{el}^{(env)} = E_{el,low}^{(env)} + E_{el,corr}^{(env)} \quad (10)$$

$$G_{pol}^{(env)} = G_{pol,low}^{(env)} + G_{pol,corr}^{(env)} \quad (11)$$

$$G_{cav}^{(env)} = G_{cav,low}^{(env)} + G_{cav,corr}^{(env)} \quad (12)$$

$$G_{es}^{(env)} = G_{es,low}^{(env)} + G_{es,corr}^{(env)} \quad (13)$$

$$G_{n/es}^{(env)} = G_{n/es,low}^{(env)} + G_{n/es,corr}^{(env)} \quad (14)$$

The remaining components of the Gibbs energy are calculated at a lower quantum level only.

Within this formalism, the solvation Gibbs energy ($\Delta G^{(solv)}$) of species X can be calculated as the difference of its Gibbs energy in solution and in the gas phase

$$\Delta G^{(solv)} = G^{(sol)} - G^{(g)} \quad (15)$$

and can be decomposed as

$$\Delta G^{(solv)} = \Delta G_{el}^{(solv)} + \Delta G_{solvent}^{(solv)} + \Delta G_{mol.mot.}^{(solv)} + \Delta(PV)^{(solv)} \quad (16)$$

In the latter equation, the components of solvation Gibbs energy can also be calculated as differences between the corresponding values in solution and in the gas phase

$$\Delta G_{el}^{(solv)} = G_{el}^{(sol)} - G_{el}^{(g)} \quad (17)$$

$$\Delta G_{\text{solvent}}^{(\text{solv})} = G_{\text{solvent}}^{(\text{sol})} = G_{\text{pol}}^{(\text{sol})} + G_{\text{cav}}^{(\text{sol})} + G_{\text{es}}^{(\text{sol})} + G_{\text{n/es}}^{(\text{sol})} \quad (18)$$

$$\Delta G_{\text{mol.mot.}}^{(\text{solv})} = G_{\text{mol.mot.}}^{(\text{sol})} - G_{\text{mol.mot.}}^{(\text{g})} \quad (19)$$

$$\Delta(PV)^{(\text{solv})} = (PV)^{(\text{sol})} - (PV)^{(\text{g})} \quad (20)$$

Results

Experimental. Rate constants, k_{MeCN} , for the reaction between AMBI and MeI in acetonitrile in the 293–323 K temperature range and at ambient pressure are presented in Table 1. Accurate second-order rate constants with a mean deviation less than 0.75% (most of them smaller than 0.50%) were obtained from conductivity data as explained above. These values are expressed in temperature-independent concentration units referred to 298.15 K. As reported before, in polyfunctional nitrogen bases, the quaternization site is the imine nitrogen (N_3).³⁰ Experimental evidence was obtained by TLC and ^1H NMR spectroscopy, in accordance with related reactions and predictions based on resonance structures for the quaternary cations that might be formed from AMBI.

The kinetic data presented in Table 1 were fitted by a least-squares procedure to both Arrhenius and Everett and Wynne-Jones⁵⁸ equations

$$\ln k = a + bT^{-1} \text{ (Arrhenius equation)} \quad (21)$$

$$\ln k = a + bT^{-1} + c \ln T \quad (22)$$

(Everett and Wynne-Jones equation)

This fitting exercise, which is illustrated in Figure 3, discloses a clear deviation from an Arrhenius behavior. From the corresponding regression coefficients and their standard errors, the Gibbs energy of activation, $\Delta^\ddagger G^\circ$, the enthalpy of activation, $\Delta^\ddagger H^\circ$, the entropy of activation, $\Delta^\ddagger S^\circ$, and respective standard errors were calculated. These quantities are presented in Table 1. The activation parameters are referred to standard states whose concentration is expressed in temperature-independent units.⁵⁹ As evidenced in Table 1, the individual enthalpic and entropic contributions can vary enormously with temperature when a non-Arrhenius fit is used. In particular, the entropy of activation, calculated from the regression coefficients of the Everett and Wynne-Jones fit, falls from an abnormal positive value ($17.3 \pm 8.6 \text{ cal mol}^{-1} \text{ K}^{-1}$) at 293.15 K to a normal negative value ($-42.1 \pm 8.6 \text{ cal mol}^{-1} \text{ K}^{-1}$) at 323.15 K. Substitution nucleophilic reactions that proceed via charge separation are expected to originate large negative $\Delta^\ddagger S^\circ$ values in polar solvents.⁶⁰ As anticipated, at the mean experimental temperature (308.15 K) both fitting equations yield similar values for the activation parameters. In reality, these values must become practically equal at the mean harmonic experimental temperature^{61–63} (307.83 K).

Computational. Different potential energy surfaces obtained for the reaction under examination are depicted in Figures 4–7. Two representations are shown in each Figure. One indicates the relative Gibbs energies ($\Delta G^{(\text{sol})}$ or $\Delta G^{(\text{g})}$) of all of the stationary species, calculated relative to the more stable species (binding complex 4) at a combined (corr + low) quantum level. The other includes additional results from IRC and conformational analyses; relative single-point Gibbs energies ($\Delta G_{\text{sp,low}}^{(\text{sol})}$ or $\Delta G_{\text{sp,low}}^{(\text{g})}$), which are calculated relative to the same reference point at a lower (low) quantum level, are also represented. In a given environment the results obtained at different quantum levels are in good agreement, reinforcing the mechanistic suggestions that can be inferred from them.

In solvent acetonitrile, potential energy surfaces for the Menshutkin reaction under examination present seven stationary points (see Figures 4 and 5). Some of them usually occur in characteristic $\text{S}_{\text{N}}2$ potential energy surfaces. They correspond to the separated reactants (AMBI + MeI), the binding complexes 2 and 3 directly connected to the transition state via the reaction coordinate (here referred to as usual binding complexes), the transition state (TS), and the separated products ($\text{AMBMe}^+ + \text{I}^-$). However, two unusual hydrogen-bonded binding complexes (binding complexes 1 and 4) were also identified. All of these complexes are characterized by a hydrogen bond between the iodine atom (I_{25}) and the N_{10} -amine group. One additional hydrogen bond, involving the H_{23} atom, was also identified for each complex ($\text{C}_{21}\text{--H}_{23}\text{--N}_3$ for binding complex 1 and $\text{C}_{21}\text{--H}_{23}\text{--I}_{25}$ for binding complex 4).

Two alternative paths seem to be possible for the end-point steps, in both sides of the energy barrier. The path represented by full lines in Figures 4 and 5 has a single diffusion-controlled step associated with it. This corresponds, in the reactants side of energy barrier, to a direct association of the separated species creating binding complex 2 and, in the products side of this barrier, to a direct dissociation of binding complex 3 creating the separated products. The other path, which is represented by dashed lines in the same Figures, has two associated steps, one for a conformational rearrangement (interconversion), the other being a diffusion-controlled step (association or dissociation). In the reactants side, the first step is an association of the separated reactants creating binding complex 1, followed by an interconversion of this species into binding complex 2. In the products side, the first step is an interconversion between binding complexes 3 and 4, followed by the dissociation of the latter species into the separated products. In principle, the first path should be preferred in the reactants side because it has no associated energy barriers. The second path is associated with two Gibbs energy barriers, which are higher for the products side because they arise from the transfer of an unbounded iodine atom between the C_{21} -methyl and the N_{10} -amine groups. These barriers are quite small (from $0.45 \text{ kcal mol}^{-1}$ (B3LYP/[6-31G(d)/LanL2DZ]) to $0.53 \text{ kcal mol}^{-1}$ (B3LYP/[6-31+G(d)/LanL2DZ]) in the reactants side and from $1.17 \text{ kcal mol}^{-1}$ (B3LYP/[6-31G(d)/LanL2DZ]) to $1.27 \text{ kcal mol}^{-1}$ (B3LYP/[6-31+G(d)/LanL2DZ]) in the products side). In the products side, this path should be preferred because binding complex 4 is the most stable species on all potential energy surfaces. At 298.15 K, binding complexes 3 and 4 and the separated products should coexist at final equilibrium (the Gibbs energy differences among these species are quite small). Because of entropic effects, raising the temperature will probably lower the equilibrium concentrations of both binding complexes relative to the separated products.

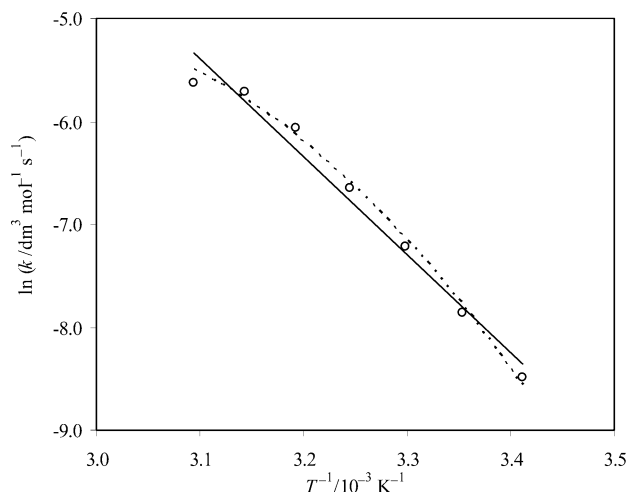
In the gas phase, it was not possible to obtain a rigorous characterization of the usual binding complexes. In fact, although the end-points of IRC analyses correspond to geometries compatible with these complexes, spontaneous conversions occur during their optimization processes creating the correspondent hydrogen-bonded complexes in both sides of the energy barrier. These interconversions are facilitated by the absence of associated energy barriers (see Figures 6 and 7).

A more detailed analysis of the components of relative Gibbs energies for all of the mentioned stationary species, carried out within the formalism developed in the previous section, is presented in Tables 2–5. These tables also include the same type of analysis for the Gibbs energy of activation, as well as

TABLE 1: Rate Constants (Mean Deviation) and Thermodynamic Functions of Activation (Standard Error) for the Quaternization Reaction between AMBI and MeI in Acetonitrile at Different Temperatures

T/K	$k_{\text{MeCN}}(\sigma k)$, $10^{-5} \text{ dm}^3 \text{ mol}^{-1} \text{ s}^{-1} \text{ }^a$	thermodynamic function of activation				
		$\Delta^\ddagger G^\circ (\sigma \Delta^\ddagger G^\circ)$, $\text{kcal mol}^{-1} \text{ }^b$	Arrhenius fit		Everett and Wynne-Jones fit	
			$\Delta^\ddagger H^\circ (\sigma \Delta^\ddagger H^\circ)$, kcal mol^{-1}	$\Delta^\ddagger S^\circ (\sigma \Delta^\ddagger S^\circ)$, $\text{cal K}^{-1} \text{ mol}^{-1} \text{ }^b$	$\Delta^\ddagger H^\circ (\sigma \Delta^\ddagger H^\circ)$, kcal mol^{-1}	$\Delta^\ddagger S^\circ (\sigma \Delta^\ddagger S^\circ)$, $\text{cal K}^{-1} \text{ mol}^{-1} \text{ }^b$
293.15	20.52 (0.07)	22.09 (0.002)	18.4 (1.3)	-12.3 (4.4)	27.2 (2.6)	17.3 (8.6)
298.15	38.51 (0.11)	22.10 (0.002)	18.4 (1.3)	-12.4 (4.4)	24.2 (1.8)	7.0 (5.9)
303.15	72.89 (0.52)	22.10 (0.004)	18.4 (1.3)	-12.4 (4.4)	21.1 (1.1)	-3.1 (3.5)
308.15	129.5 (0.3)	22.12 (0.001)	18.4 (1.3)	-12.4 (4.4)	18.1 (0.7)	-13.1 (2.4)
313.15	233.0 (1.2)	22.13 (0.003)	18.4 (1.3)	-12.5 (4.4)	15.0 (1.2)	-22.9 (3.8)
318.15	330.9 (0.6)	22.27 (0.001)	18.3 (1.3)	-12.5 (4.4)	12.0 (1.9)	-32.6 (6.1)
323.15	360.1 (1.6)	22.57 (0.003)	18.3 (1.3)	-12.5 (4.4)	8.9 (2.7)	-42.1 (8.6)

^a Rate constants are expressed in temperature-independent units. ^b Referred to standard states containing 1 mol dm⁻³ at 298.15 K.

**Figure 3.** Temperature dependence of rate constants for the quaternization reaction between AMBI and MeI in acetonitrile according to Arrhenius equation (full line) and to Everett and Wynne-Jones equation (dashed line).

a comparison to the experimental value obtained in this work for the present Menshutkin reaction in acetonitrile.

In solution, the electronic Gibbs energies ($\Delta G_{\text{el}}^{\text{(sol)}}$) favored binding complexes BC₁ and BC₄ stabilized by hydrogen bonds between the iodine atom (I₂₅) and the N₁₀-amine group. The component of the Gibbs energy associated with the solvent ($\Delta G_{\text{solvent}}^{\text{(sol)}}$) preferentially stabilizes the more polar species (the transition state and the species in the products side of the energy barrier are favored relative to the species in the reactants side) and with larger solvent-accessible areas (the usual complexes are favored relative to the hydrogen-bonded complexes and the separated species are favored relative to the dimers). The component the Gibbs energy associated with molecular motions ($\Delta G_{\text{mol.mot.}}^{\text{(sol)}}$) favored separated species relative to the corresponding dimers. In fact, the association of a separated species creating a dimer involves the conversion of six high-entropy (translational and rotational) normal modes into six (or five for the transition state) less entropic vibrational modes. The $\Delta(PV)^{\text{(sol)}}$ component has a significantly less marked effect in the opposite direction (dimers are favored relative to separated species). Values for activation Gibbs energies, calculated at both quantum levels, are in good agreement with the experimental value obtained in this work. Their components reflect the general trends discussed above. In fact, both the electronic and molecular motion components increase activation Gibbs energies, while the other components have the opposite effect.

In the gas phase, the Gibbs energy component associated with the solvent does not exist and the other components have a similar behavior as in acetonitrile. In fact, electronic Gibbs

energies ($\Delta G_{\text{el}}^{\text{(g)}}$) favored the hydrogen-bonded binding complexes, the Gibbs energy component associated with molecular motions ($\Delta G_{\text{mol.mot.}}^{\text{(g)}}$) favored separated species relative to dimers, and the $\Delta(PV)^{\text{(sol)}}$ component has a less marked effect in the opposite direction. If only the electronic component is considered, a characteristic double-well energy profile would be obtained. However, in the global Gibbs energy profile the separated reactants are more stable than binding complex 1. Activation Gibbs energies in the gas phase are significantly higher than the corresponding values in acetonitrile. This is consistent with a transition state characteristic of the Menshutkin reaction,^{42,64} which is more polar than the separated reactants (see Figure 1).

The components of the solvation Gibbs energy for the common stationary species identified on the potential energy surfaces of the reaction under study in both the gas phase and acetonitrile are presented in Tables 6 and 7. The analysis of these results enables us to conclude that the electronic component ($\Delta G_{\text{el}}^{\text{(sol)}}$) does not usually favor the solvation process. In fact, this component is associated with the unfavored effects of solute polarization and conformational rearrangement. The transition state is the species less destabilized (or even lightly stabilized at the B3LYP/[6-311++G(3df,3pd)/LanL2DZ]//B3LYP/[6-31G(d)/LanL2DZ] level) by this type of effects. The solvent-associated component ($\Delta G_{\text{solvent}}^{\text{(sol)}}$) usually favors the solvation process because the attractive (electrostatic and nonelectrostatic) solute-solvent interactions compensate for the work done on solvent reorganization (polarization and cavitation). The only exception occurs for binding complex 1, where the repulsive solvent reorganization terms are predominant. The molecular motion ($\Delta G_{\text{mol.mot.}}^{\text{(sol)}}$) and $\Delta(PV)^{\text{(sol)}}$ components lightly favor the solvated relative to the gas phase species. In general, the solvation process stabilizes preferentially the species more polar and with larger solvent-accessible areas. In this context, activation Gibbs energies are decreased by both electronic and solvent-associated effects.

The AIM analysis, performed for binding complexes 1 and 4, confirmed the occurrence of two hydrogen bonds for each structure. In fact, bond critical points (bcp) were identified between atoms I₂₅ and H₁₇ for both complexes, between H₂₃ and N₃ for binding complex 1, and between H₂₃ and I₂₅ for binding complex 4. The charge ($\rho(r)$) and energy ($H(r)$) densities obtained in these bcp are presented in Table 8. These values can be used as an index to evaluate the strength of the corresponding hydrogen bonds.^{65,66} The conjugation of an increase in $\rho(r)$ values with a decrease in the $H(r)$ negative values indicates an increase of charge density in the bonding region and therefore in the strength of the hydrogen bond. The results obtained in AIM analysis were compared to relevant

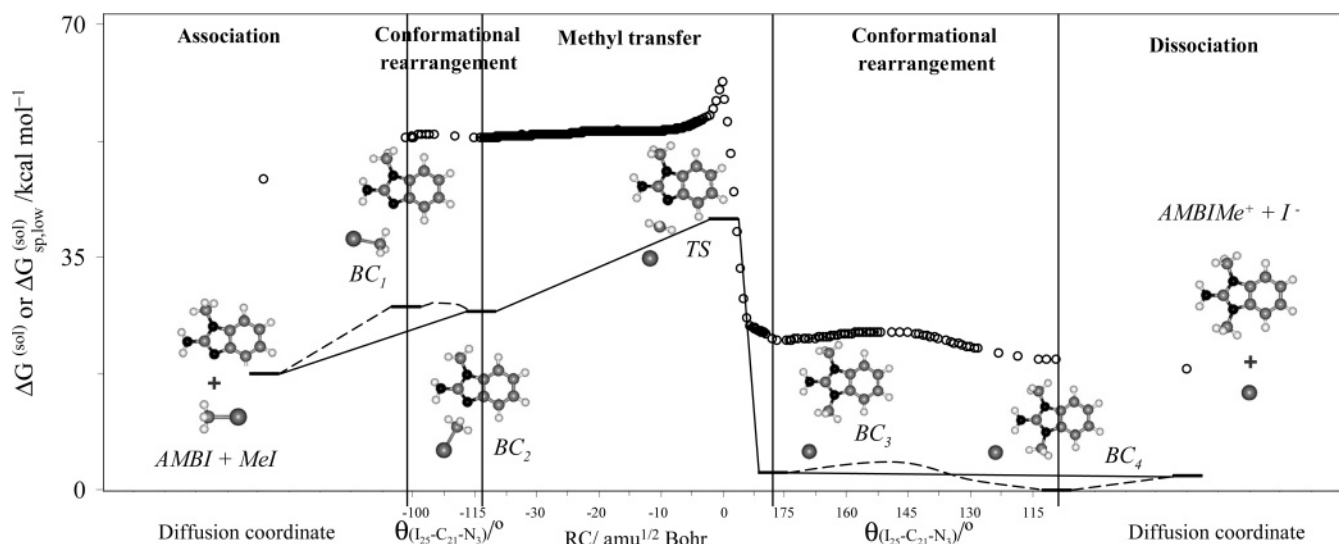


Figure 4. Gibbs energy profile for the quaternization reaction between 2-amino-1-methylbenzimidazole (AMBI) and iodomethane (MeI) in acetonitrile, calculated at a B3LYP/[6-311++G(3df,3pd)/LANL2DZ]/B3LYP/[6-31G(d)/LANL2DZ] level. All of the stationary species are identified (AMBI + MeI = separated reactants, BC₁ = binding complex 1, BC₂ = binding complex 2, BC₃ = binding complex 3, BC₄ = binding complex 4, TS = transition state, AMBIME⁺ + I⁻ = separated products). The relative Gibbs energies ($\Delta G^{(sol)}$) of all of the stationary points, calculated relative to the more stable one (BC₄) at a B3LYP/[6-311++G(3df,3pd)/LANL2DZ]/B3LYP/[6-31G(d)/LANL2DZ] level, are represented by horizontal strokes (—). The relative single-point Gibbs energies ($\Delta G_{sp,low}^{(sol)}$) of all of the nonstationary (obtained from the IRC and conformational analyses) and stationary points, calculated relative to the same reference at a B3LYP/[6-31G(d)/LANL2DZ] level, are also represented using circles (○○○).

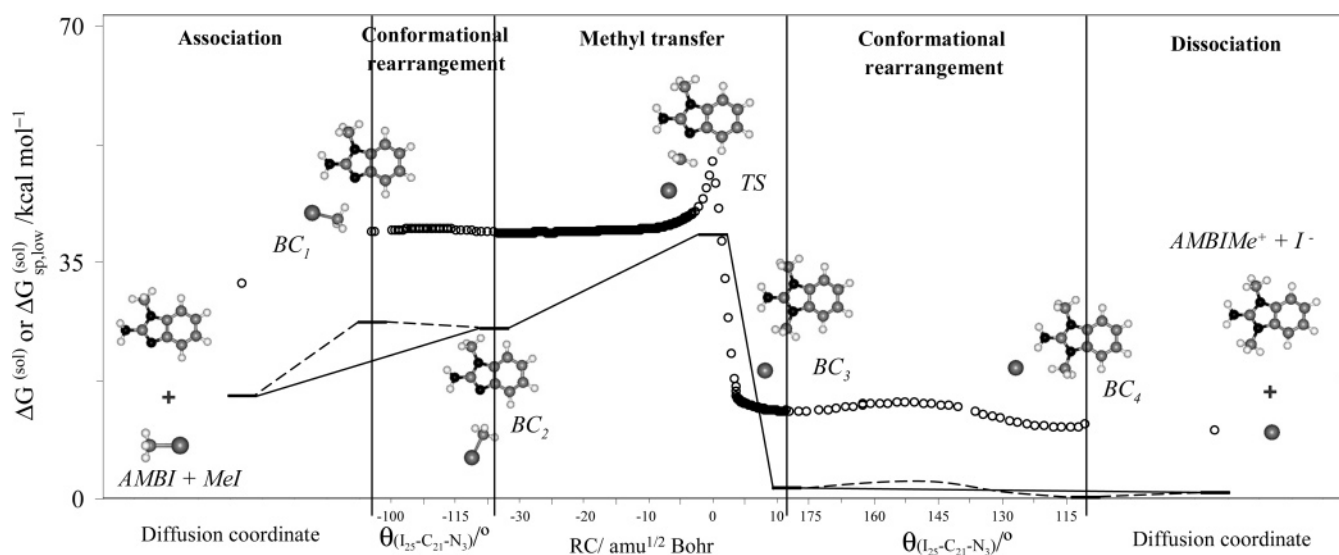


Figure 5. Gibbs energy profile for the quaternization reaction between 2-amino-1-methylbenzimidazole (AMBI) and iodomethane (MeI) in acetonitrile, calculated at a B3LYP/[6-311++G(3df,3pd)/LANL2DZ]/B3LYP/[6-31+G(d)/LANL2DZ] level. All of the stationary species are identified (AMBI + MeI = separated reactants, BC₁ = binding complex 1, BC₂ = binding complex 2, BC₃ = binding complex 3, BC₄ = binding complex 4, TS = transition state, AMBIME⁺ + I⁻ = separated products). The relative Gibbs energies ($\Delta G^{(sol)}$) of all of the stationary points, calculated relative to the more stable one (BC₄) at a B3LYP/[6-311++G(3df,3pd)/LANL2DZ]/B3LYP/[6-31+G(d)/LANL2DZ] level, are represented by horizontal strokes (—). The relative single-point Gibbs energies ($\Delta G_{sp,low}^{(sol)}$) of all of the nonstationary (obtained from the IRC and conformational analyses) and stationary points, calculated relative to the same reference at a B3LYP/[6-31+G(d)/LANL2DZ] level, are also represented using circles (○○○).

geometric parameters associated with the hydrogen bonds presented in Tables 9 and 10. In this context, the following tendencies can be inferred: The I₂₅–H₁₇ hydrogen bond should be stronger in binding complex 4 than in binding complex 1. This is consistent with the larger intrinsic stability of the former species (compare the relative values of the electronic Gibbs energies in Tables 2–5), with hydrogen bond distances that are systematically shorter for the former complex, and with the charge separation between the atoms involved in both complexes.

The I₂₅–H₁₇ hydrogen bond in binding complex 4 should be stronger than the other two hydrogen bonds, the strength of the latter being very similar. However, the opposite behavior should

be expectable for the former hydrogen bond in binding complex 1. This is consistent with the charge separation between the atoms involved in the different hydrogen bonds and with the corresponding hydrogen bond distances.

The solvent destabilizes all of the hydrogen bonds, which can be confirmed by both the AIM indexes and the hydrogen-bond distances. This effect is more pronounced in binding complex 4 than in binding complex 1. This is consistent with a stronger interaction of the former complex with the solvent (compare the relative values of the component of the Gibbs energies associated with the solvent in Tables 2, 3, 6, and 7).

We were able to achieve a detailed description of solvent participation in the reaction coordinate of this complex system

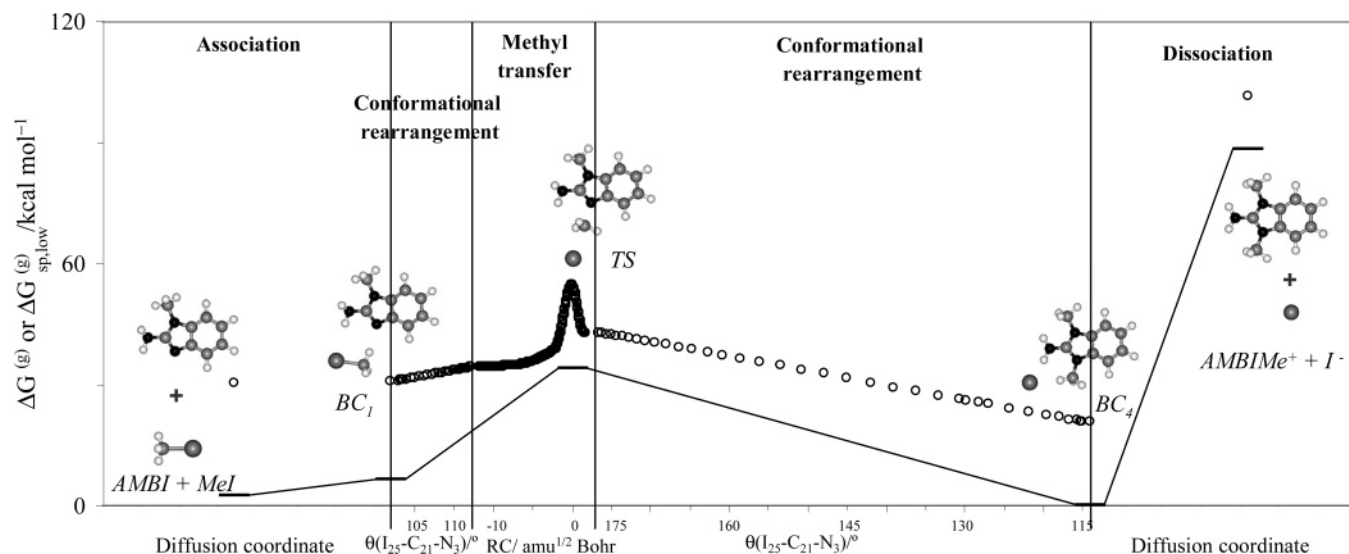


Figure 6. Gibbs energy profile for the quaternization reaction between 2-amino-1-methylbenzimidazole (AMBI) and iodomethane (MeI) in the gas phase, calculated at a B3LYP/[6-311++G(3df,3pd)/LANL2DZ]/B3LYP/[6-31G(d)/LANL2DZ] level. All of the stationary species are identified (AMBI + MeI = separated reagents, BC₁ = binding complex 1, BC₄ = binding complex 4, TS = transition state, AMBIMe⁺ + I⁻ = separated products). The relative Gibbs energies ($\Delta G^{(g)}$) of all of the stationary points, calculated relative to the more stable one (BC₄) at a B3LYP/[6-311++G(3df,3pd)/LANL2DZ]/B3LYP/[6-31G(d)/LANL2DZ] level, are represented by horizontal strokes (—). The relative single-point Gibbs energies ($\Delta G_{sp,low}^{(g)}$) of all of the nonstationary (obtained from the IRC and conformational analyses) and stationary points, calculated relative to the same reference at a B3LYP/[6-31G(d)/LANL2DZ] level, are also represented using circles (○○○).

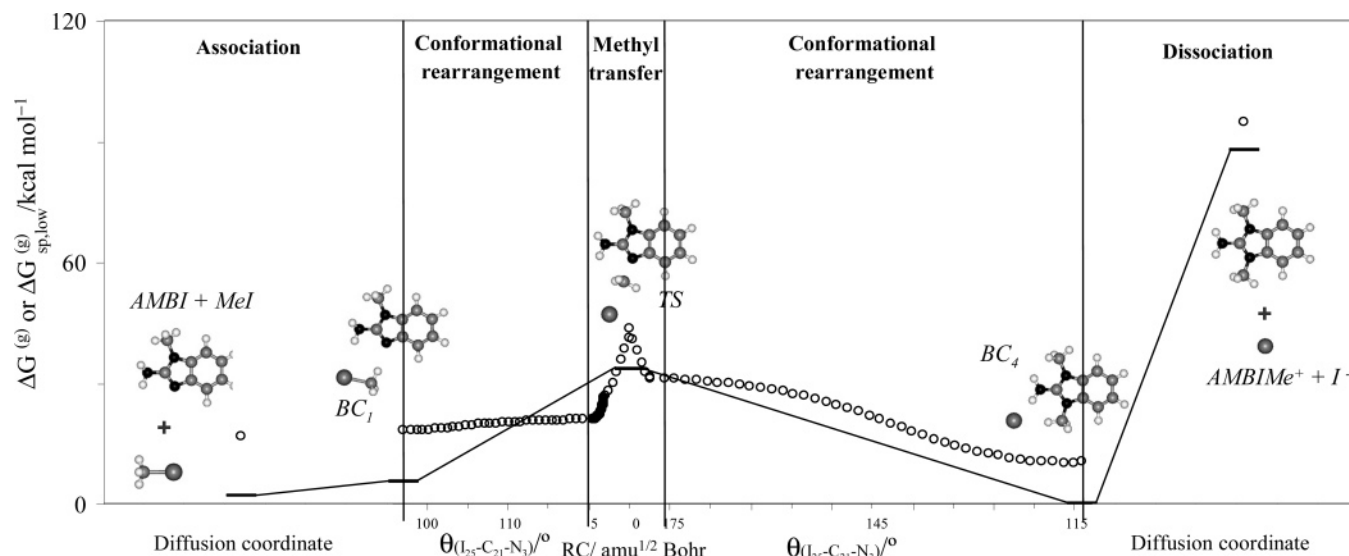


Figure 7. Gibbs energy profile for the quaternization reaction between 2-amino-1-methylbenzimidazole (AMBI) and iodomethane (MeI) in the gas phase, calculated at a B3LYP/[6-311++G(3df,3pd)/LANL2DZ]/B3LYP/[6-31+G(d)/LANL2DZ] level. All of the stationary species are identified (AMBI + MeI = separated reagents, BC₁ = binding complex 1, BC₄ = binding complex 4, TS = transition state, AMBIMe⁺ + I⁻ = separated products). The relative Gibbs energies ($\Delta G^{(g)}$) of all of the stationary points, calculated relative to the more stable one (BC₄) at a B3LYP/[6-311++G(3df,3pd)/LANL2DZ]/B3LYP/[6-31+G(d)/LANL2DZ] level, are represented by horizontal strokes (—). The relative single-point Gibbs energies ($\Delta G_{sp,low}^{(g)}$) of all of the nonstationary (obtained from the IRC and conformational analyses) and stationary points, calculated relative to same reference at a B3LYP/[6-31+G(d)/LANL2DZ] level, are also represented using circles (○○○).

using the PCM. This model, which represents the solvent as a continuum polarizable medium, is specially appropriated to describe the solute–solvent interactions in aprotic environments. However, fine details of solvent effects at an atomistic level in different complex reacting systems can probably be revealed using recent methods that combine discrete and continuum descriptions of the solvent.^{67,68}

For all stationary species including the 2-amino-1-methylbenzimidazole pattern (AMBI, binding complexes, transition state and AMBIMe⁺), two isomers associated with the rotation of the N₁₀-amine group were identified. In fact, dihedral angles

(H₁₆–N₁₀–C₂–N₃) and (H₁₇–N₁₀–C₂–N₃), together with other correlated dihedral angles, show almost symmetric values for these two isomeric forms and the respective energy difference is close to zero. The most relevant parameters are presented in Tables 9 and 10. The analysis of the geometrical parameters associated with the C₂₁-methyl group and the iodine atom (I₂₅) allows the characterization of the different stationary species. In particular, it can be observed in Tables 9 and 10 that the iodomethane molecule and the 2-amino-1-methylbenzimidazole ring are clearly noncoplanar in binding complex 2, whereas the other species adopt near-coplanar conformations. This is

TABLE 2: Relative Gibbs Energies ($\Delta G^{(\text{sol})}$) and Their Components in kcal mol⁻¹ for All of the Stationary Species Identified on the Potential Energy Surface for the Quaternization Reaction between 2-Amino-1-methylbenzimidazole and Iodomethane in Acetonitrile, Calculated Relative to the More Stable One (Binding Complex 4) at a B3LYP/[6-311++G(3df,3pd)/LANL2DZ]/B3LYP/[6-31G(d)/LANL2DZ] Level^a

stationary species	$\Delta G_{\text{el}}^{(\text{sol})}$	$\Delta G_{\text{solvent}}^{(\text{sol})}$	$\Delta G_{\text{mol.mot.}}^{(\text{sol})}$	$\Delta(PV)^{(\text{sol})}$	$\Delta G^{(\text{sol})}$
separated reactants	7.14	19.08	-9.70	0.02	16.54
binding complex 1	1.65	26.40	-0.99	0.00	27.05
binding complex 2	5.33	22.33	-1.39	0.00	26.28
transition state	25.62	14.15	0.58	0.00	40.35
activation	18.48	-4.93	10.28	-0.02	23.81
activation (exptl)					22.11
binding complex 3	22.79	-20.07	-0.61	0.00	2.11
binding complex 4	0.00	0.00	0.00	0.00	0.00
separated products	86.28	-81.19	-3.87	0.02	1.24

^a Theoretical and experimental values of the activation Gibbs energy at 298.15 K are also presented.

TABLE 3: Relative Gibbs Energies ($\Delta G^{(\text{sol})}$) and Their Components in kcal mol⁻¹ for All of the Stationary Species Identified on the Potential Energy Surface for the Quaternization Reaction between 2-Amino-1-methylbenzimidazole and Iodomethane in Acetonitrile, Calculated Relative to the More Stable One (Binding Complex 4) at a B3LYP/[6-311++G(3df,3pd)/LANL2DZ]/B3LYP/[6-31+G(d)/LANL2DZ] Level^a

stationary species	$\Delta G_{\text{el}}^{(\text{sol})}$	$\Delta G_{\text{solvent}}^{(\text{sol})}$	$\Delta G_{\text{mol.mot.}}^{(\text{sol})}$	$\Delta(PV)^{(\text{sol})}$	$\Delta G^{(\text{sol})}$
separated reactants	7.36	18.78	-11.70	0.02	14.46
binding complex 1	1.86	26.31	-1.92	0.00	26.25
binding complex 2	4.12	23.39	-2.35	0.00	25.15
transition state	26.83	12.99	-0.70	0.00	39.12
activation	19.47	-5.79	11.00	-0.02	24.66
activation (exptl)					22.11
binding complex 3	22.39	-19.66	-1.16	0.00	1.57
binding complex 4	0.00	0.00	0.00	0.00	0.00
separated products	86.36	-81.23	-4.25	0.02	0.91

^a Theoretical and experimental values of the activation Gibbs energy at 298.15 K are also presented.

TABLE 4: Relative Gibbs Energies ($\Delta G^{(\text{g})}$) and Their Components in kcal mol⁻¹ for All of the Stationary Species Identified on the Potential Energy Surface for the Quaternization Reaction between 2-Amino-1-methylbenzimidazole and Iodomethane in the Gas Phase, Calculated Relative to the More Stable Species (Binding Complex 4) at a B3LYP/[6-311++G(3df,3pd)/LANL2DZ]/B3LYP/[6-31G(d)/LANL2DZ] Level^a

stationary species	$\Delta G_{\text{el}}^{(\text{g})}$	$\Delta G_{\text{mol.mot.}}^{(\text{g})}$	$\Delta(PV)^{(\text{g})}$	$\Delta G^{(\text{g})}$
separated reactants	12.46	-10.61	0.59	2.44
binding complex 1	8.33	-2.30	0.00	6.03
transition state	34.15	-0.63	0.00	33.51
activation	21.69	9.97	-0.59	31.07
binding complex 4	0.00	0.00	0.00	0.00
separated products	92.36	-4.90	0.59	88.06

^a The theoretical value of the activation Gibbs energy is also presented.

consistent with the formation of late transition states in acetonitrile because their structures are more similar to binding complex 3 than to binding complex 2.

Turning attention to the effect of changing solvent, we note that the reaction under examination in acetonitrile was studied previously in methanol for the same temperature range by some of the present authors³⁰ and a good Arrhenius fit was observed for the kinetic data ($\ln(k_{\text{MeOH}})$ against $1/T$). Kondo and his associates have paid much attention to the different solvating ability of acetonitrile, methanol, and their binary mixtures in a

TABLE 5: Relative Gibbs Energies ($\Delta G^{(\text{g})}$) and Their Components in kJ mol⁻¹ for All of the Stationary Species Identified on the Potential Energy Surface for the Quaternization Reaction between 2-Amino-1-methylbenzimidazole and Iodomethane in the Gas Phase, Calculated Relative to the More Stable One (Binding Complex 4) at a B3LYP/[6-311++G(3df,3pd)/LANL2DZ]/B3LYP/[6-31+G(d)/LANL2DZ] Level^a

stationary species	$\Delta G_{\text{el}}^{(\text{g})}$	$\Delta G_{\text{mol.mot.}}^{(\text{g})}$	$\Delta(PV)^{(\text{g})}$	$\Delta G^{(\text{g})}$
separated reactants	12.35	-10.89	0.59	2.05
binding complex 1	8.20	-2.86	0.00	5.34
transition state	34.09	-0.89	0.00	33.19
activation	21.74	10.00	-0.59	31.14
binding complex 4	0.00	0.00	0.00	0.00
separated products	92.34	-5.47	0.59	87.46

^a The theoretical value of the activation Gibbs energy is also presented.

TABLE 6: Solvation Gibbs Energies ($\Delta G^{(\text{sol})}$) and Their Components in kcal mol⁻¹ for the Common Stationary Species Identified on the Potential Energy Surface for the Quaternization Reaction between 2-Amino-1-methylbenzimidazole and Iodomethane in Both the Gas Phase and Acetonitrile, Calculated at a B3LYP/[6-311++G(3df,3pd)/LANL2DZ]/B3LYP/[6-31G(d)/LANL2DZ] Level^a

stationary species	$\Delta G_{\text{el}}^{(\text{sol})}$	$\Delta G_{\text{solvent}}^{(\text{sol})}$	$\Delta G_{\text{mol.mot.}}^{(\text{sol})}$	$\Delta(PV)^{(\text{sol})}$	$\Delta G^{(\text{sol})}$
separated reactants	3.04	-4.86	-0.86	-1.14	-3.81
binding complex 1	1.68	2.46	-0.46	-0.57	3.12
transition state	-0.16	-9.79	-0.55	-0.57	-11.07
activation	-3.20	-4.93	0.30	0.57	-7.26
binding complex 4	8.36	-44.01	-1.76	-0.57	-17.91
separated products	2.28	-105.13	-0.73	-1.14	-40.30

^a The solvation effect on the theoretical value of the activation Gibbs energy is also presented.

TABLE 7: Solvation Gibbs Energies ($\Delta G^{(\text{sol})}$) and Their Components in kcal mol⁻¹ for the Common Stationary Species Identified on the Potential Energy Surfaces for the Quaternization Reaction between 2-Amino-1-methylbenzimidazole and Iodomethane in Both the Gas Phase and Acetonitrile, Calculated at a B3LYP/[6-311++G(3df,3pd)/LANL2DZ]/B3LYP/[6-31+G(d)/LANL2DZ] Level^a

stationary species	$\Delta G_{\text{el}}^{(\text{sol})}$	$\Delta G_{\text{solvent}}^{(\text{sol})}$	$\Delta G_{\text{mol.mot.}}^{(\text{sol})}$	$\Delta(PV)^{(\text{sol})}$	$\Delta G^{(\text{sol})}$
separated reactants	3.31	-5.11	-2.48	-1.14	-5.41
binding complex 1	1.96	2.42	-0.72	-0.57	3.09
transition state	1.04	-10.90	-1.47	-0.57	-11.90
activation	-2.27	-5.79	1.01	0.57	-6.48
binding complex 4	8.30	-43.55	-1.67	-0.57	-17.82
separated products	2.32	-105.12	-0.44	-1.14	-39.96

^a The solvation effect on the theoretical value of the activation Gibbs energy is also presented.

variety of Menshutkin reactions.^{69–72} They have ascribed part of this difference to hydrogen-bonding interactions between methanol and nucleophile molecules containing nitrogen atoms. Owing to these specific interactions, a given Menshutkin reaction is much slower in methanol than in acetonitrile, which is a dipolar aprotic solvent of similar ionizing power. Indeed, methanol is an amphiprotic hydroxylic solvent, whereas acetonitrile is an aprotic protophobic solvent that possesses poor solvating properties for anions with localized charges, as is the case of iodide ions.⁷³ However, no deviating Arrhenius behavior has been reported for quaternization reactions in acetonitrile. Therefore, we need to investigate the main reasons responsible for the different temperature effects observed in the two solvents. To this end, $\ln(k_{\text{MeCN}}/k_{\text{MeOH}})$ was represented against $1/T$ (see Figure 8).

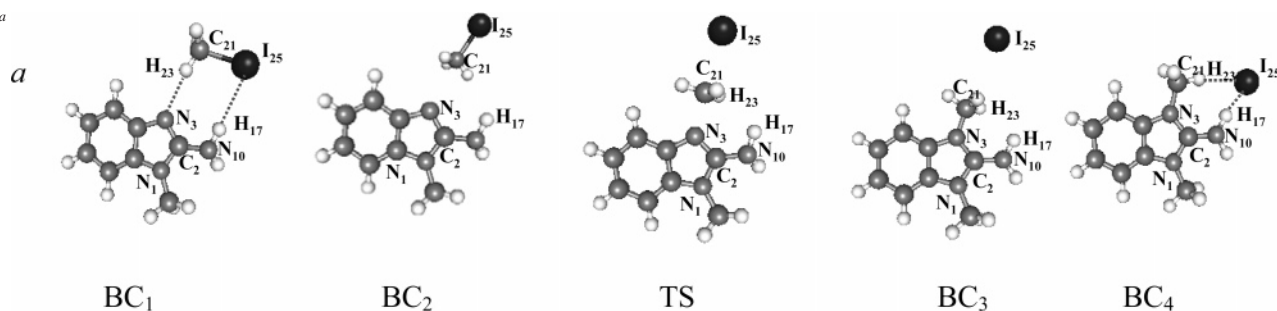
TABLE 8: Charge ($\rho(r)$) and Energy ($H(r)$) Densities Calculated for Bond Critical Points Associated with Hydrogen Bonds

stationary species	environment	quantum level	H ₁₇ –I ₂₅		H ₂₃ –N ₃		H ₂₃ –I ₂₅	
			$\rho(r)$	$H(r)$	$\rho(r)$	$H(r)$	$\rho(r)$	$H(r)$
binding complex 1	vacuum	level 1 ^a	0.00745	–0.00370	0.01433	–0.00923		
binding complex 1	acetonitrile	level 1 ^a	0.00657	–0.00330	0.01316	–0.00832		
binding complex 1	vacuum	level 2 ^b	0.00738	–0.00366	0.01207	–0.00755		
binding complex 1	acetonitrile	level 2 ^b	0.00642	–0.00322	0.01024	–0.00620		
binding complex 4	vacuum	level 1 ^a	0.03505	–0.01467			0.01430	–0.00699
binding complex 4	acetonitrile	level 1 ^a	0.017561	–0.00849			0.00905	–0.00446
binding complex 4	vacuum	level 2 ^b	0.03564	–0.01494			0.01386	–0.00677
binding complex 4	acetonitrile	level 2 ^b	0.01800	–0.00873			0.00930	–0.00460

^a B3LYP/[6-311++G(3df,3pd)/LanL2DZ]/B3LYP/[6-31G(d)/LanL2DZ]. ^b B3LYP/[6-311++G(3df,3pd)/LanL2DZ]/B3LYP/[6-31+G(d)/LanL2DZ].

TABLE 9: Most Relevant Geometrical Parameters Obtained for the Stationary Species (BC₁ = Binding Complex 1, BC₂ = Binding Complex 2, BC₃ = Binding Complex 3, BC₄ = Binding Complex 4, TS = Transition State) at a B3LYP/[6-311++G(3df,3pd)/LanL2DZ]/B3LYP/[6-31G(d)/LanL2DZ] Level

stationary species ^a	BC ₁		BC ₂		TS		BC ₃		BC ₄	
environment	solution	vacuum	solution		solution	vacuum	solution		solution	vacuum
bond length										
C ₂₁ –N ₃	3.46	3.41	3.59		2.19	1.94	1.46		1.46	1.47
I ₂₅ –C ₂₁	2.20	2.20	2.20		2.60	2.79	3.85		4.14	3.90
I ₂₅ –H ₁₇	3.11	3.06							2.65	2.33
H ₂₃ –N ₃	2.38	2.33								
I ₂₅ –H ₂₃									3.06	2.82
bond angle										
C ₂₁ –N ₃ –C ₂	125.1	124.3	99.4		126.9	123.6	125.0		127.1	126.9
I ₂₅ –C ₂₁ –N ₃	99.1	99.7	114.8		179.7	177.5	174.9		107.1	104.6
I ₂₅ –H ₁₇ –N ₁₀	172.6	171.5							167.1	172.1
C ₂₁ –H ₂₃ –N ₃	170.0	170.4								
I ₂₅ –H ₂₃ –C ₂₁									174.8	169.7
dihedral angle										
C ₂₁ –N ₃ –C ₂ –N ₁	–172.0	–173.4	–113.0		–173.3	–173.8	–179.4		176.1	177.4
I ₂₅ –C ₂₁ –N ₃ –C ₂	–7.4	–0.9	–115.3		–14.5	5.3	9.6		20.4	21.1

^a

According to the transition state theory, this representation can be expressed by the following equation

$$\ln(k_{\text{MeCN}}/k_{\text{MeOH}}) = -\frac{\Delta\Delta^\ddagger H_{\text{MeOH} \rightarrow \text{MeCN}}^\circ}{R} \frac{1}{T} + \frac{\Delta\Delta^\ddagger S_{\text{MeOH} \rightarrow \text{MeCN}}^\circ}{R} \quad (23)$$

where

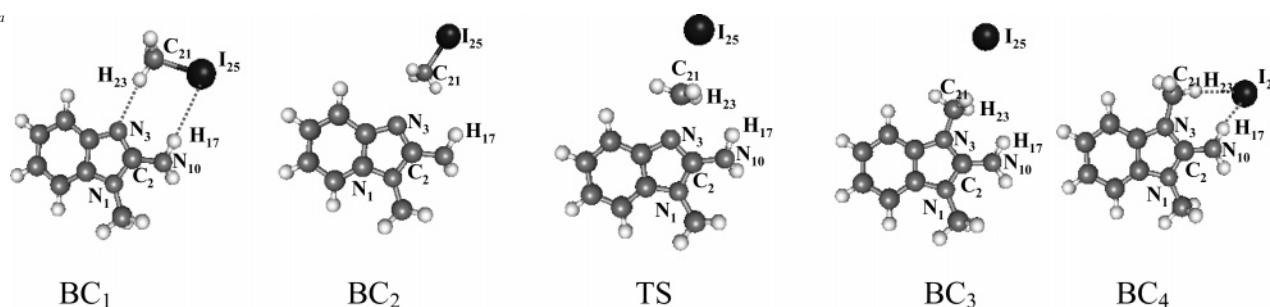
$$\begin{aligned} \Delta\Delta^\ddagger H_{\text{MeOH} \rightarrow \text{MeCN}}^\circ &= \Delta^\ddagger H_{\text{MeCN}}^\circ - \Delta^\ddagger H_{\text{MeOH}}^\circ \text{ and} \\ \Delta\Delta^\ddagger S_{\text{MeOH} \rightarrow \text{MeCN}}^\circ &= \Delta^\ddagger S_{\text{MeCN}}^\circ - \Delta^\ddagger S_{\text{MeOH}}^\circ \end{aligned} \quad (24)$$

If an Arrhenius behavior was observed for both environments, then a linear plot of $\ln(k_{\text{MeCN}}/k_{\text{MeOH}})$ against $1/T$ should be obtained. A positive slope is expected because acetonitrile is more polar than methanol, leading to a negative value for $\Delta\Delta^\ddagger H_{\text{MeOH} \rightarrow \text{MeCN}}^\circ$. Moreover, $\Delta\Delta^\ddagger H_{\text{MeOH} \rightarrow \text{MeCN}}^\circ$ and $\Delta\Delta^\ddagger S_{\text{MeOH} \rightarrow \text{MeCN}}^\circ$ should be nearly temperature independent.

In Figure 8, an Arrhenius behavior is observed only at high experimental temperatures. The quite small temperature range investigated cannot explain this anomaly based on a strong dependence of $\Delta\Delta^\ddagger H_{\text{MeOH} \rightarrow \text{MeCN}}^\circ$ and $\Delta\Delta^\ddagger S_{\text{MeOH} \rightarrow \text{MeCN}}^\circ$ on temperature. We seek an explanation in terms of the role played

TABLE 10: Most Relevant Geometrical Parameters Obtained for the Stationary Species (BC₁ = Binding Complex 1, BC₂ = Binding Complex 2, BC₃ = Binding Complex 3, BC₄ = Binding Complex 4, TS = Transition State) at a B3LYP/[6-311++G(3df,3pd)/LanL2DZ]/[B3LYP/[6-31+G(d)/LanL2DZ] Level

stationary species ^a	BC ₁		BC ₃	TS		BC ₃	BC ₄	
	solution	vacuum	solution	solution	vacuum	solution	solution	vacuum
bond length								
C ₂₁ –N ₃	3.57	3.49	3.72	2.17	1.94	1.46	1.46	1.47
I ₂₅ –C ₂₁	2.19	2.19	2.19	2.62	2.79	3.80	4.13	3.90
I ₂₅ –H ₁₇	3.12	3.06					2.63	2.32
H ₂₃ –N ₃	2.50	2.41						
I ₂₅ –H ₂₃							3.04	2.83
bond angle								
C ₂₁ –N ₃ –C ₂	124.0	124.0	150.4	127.2	123.8	124.6	127.2	126.6
I ₂₅ –C ₂₁ –N ₃	97.5	98.4	122.7	179.8	177.5	174.6	107.7	102.1
I ₂₅ –H ₁₇ –N ₁₀	173.4	173.7					167.6	170.3
C ₂₁ –H ₂₃ –N ₃	167.4	168.3						
I ₂₅ –H ₂₃ –C ₂₁							175.8	165.6
dihedral angle								
C ₂₁ –N ₃ –C ₂ –N ₁	–169.8	–175.5	–163.1	–177.6	–175.4	–179.2	175.8	176.0
I ₂₅ –C ₂₁ –N ₃ –C ₂	–8.7	–2.2	–17.3	9.7	3.5	11.5	18.6	28.0

^a

by nonreacting nitrogen atoms in polyfunctional substrates, which has been noticed already by Kondo et al.⁷¹ with respect to solute–solvent interactions. We believe that lowering the temperature will affect the interplay of cooperative and opposing interactions between acetonitrile and nonreacting nitrogen atoms in AMBI. An alternative mechanistic-based interpretation can thus be proposed. As mentioned above, the separated products and binding complexes BC₃ and BC₄ should coexist in acetonitrile at low temperatures, whereas the separated products are probably favored at high temperatures by entropic effects in this solvent. Otherwise, the protic nature of solvent methanol probably favors the separated products relative to the binding complexes. In fact, in the former species the most polar groups are less sterically hindered and, hence, abler than binding

complexes to form hydrogen bonds with the solvent. The quantity $\ln(k_{\text{MeCN}}/k_{\text{MeOH}})$ presents an Arrhenius positive slope at high experimental temperatures, probably because a single-step mechanism ($\text{AMBI} + \text{MeI} \rightleftharpoons \text{TS} \rightarrow \text{AMBIME}^+ + \text{I}^-$) is common to both environments and the basic assumptions of the transition state theory underpinning eq 23 are verified. At low experimental temperatures, the same behavior would be expected for methanol, whereas a more complex mechanism ($\text{AMBI} + \text{MeI} \rightarrow \text{BC}_2 \rightleftharpoons \text{TS} \rightarrow \text{BC}_3 \rightarrow \text{BC}_4 \rightarrow \text{AMBIME}^+ + \text{I}^-$) should occur in acetonitrile. This explains why the relative formation of the separated products in acetonitrile relative to methanol is significantly lower than the predictions obtained using an Arrhenius model. Then our explanation is specific to a particular choice for the nucleophile–solvent pair.

Conclusions

The quaternization reaction between 2-amino-1-methylbenzimidazole and iodomethane has been studied using experimental and theoretical approaches. The results obtained by both approaches are in excellent agreement and allow us to propose a mechanism consistent with the general features of a S_N2 reaction. In particular, it has been confirmed that solvent acetonitrile decreases the activation Gibbs energy in relation to the barrier in the gas phase. This is an expected result for a Menshutkin reaction in which the transition state is more polar than the separated reactants (see Figure 1b). However, the mechanism proposed in this work presents some novelty arising from the participation of the N₁₀-amine group adjacent to the nucleophilic nitrogen (N₃). On one hand, two unusual hydrogen-bonded binding complexes, which are located in different sides of the energy barrier, have been identified. In the gas phase, the usual binding complexes are probably metastable, being substituted by the new unusual species in the characteristic

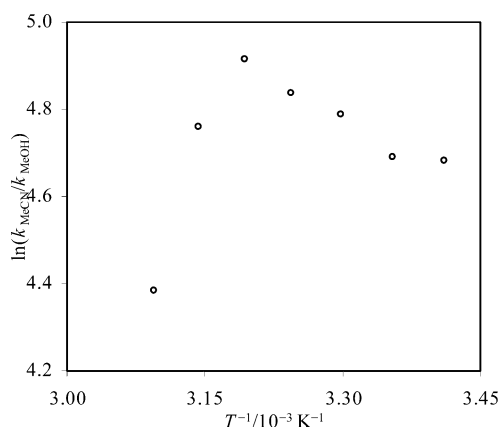


Figure 8. Plot of $\ln(k_{\text{MeCN}}/k_{\text{MeOH}})$ vs $1/T$, where k_{MeCN} and k_{MeOH} are, respectively, the rate constants in acetonitrile and methanol, for the quaternization reaction between 2-amino-1-methylbenzimidazole and iodomethane.

double-well energy profiles. In acetonitrile, both types of complexes probably coexist at ambient temperature and two different paths have been proposed for the end-point steps of the mechanism. On the other hand, the rotation of the N₁₀-amine group is suggested to originate two isomeric forms for all stationary species that occur on the potential energy surfaces. A topological analysis of the electronic density, carried out with the AIM formalism, reinforced some of the previous conclusions and provided further insight into characteristics of the hydrogen bonds identified in binding complexes 1 and 4.

The contribution of acetonitrile in the reaction coordinate was detected using the polarizable continuum model for solvent effects. It will thus be of interest to examine the role played by solvent molecules in complex reacting systems using recent solvation models that combine discrete and continuum representations of the solvent.^{67,68}

A non-Arrhenius behavior has been found experimentally for the effect of temperature on the rate constants of this Menshutkin reaction in acetonitrile, although this effect was reported to be well behaved in solvent methanol. The formation of acetonitrile-induced novel binding complexes is possibly at the origin of this abnormal temperature dependence, with reaction rates being much slower at low temperatures than expected by extrapolation from values at high temperature. Underlying these interesting solvent and temperature effects on a Menshutkin reaction is the choice of 2-amino-1-methylbenzimidazole as the nucleophile, which is an organic molecule containing three nitrogen atoms.

Acknowledgment. Financial support from Fundação para a Ciência e a Tecnologia (FCT), projects POCTI/QUI/55673/2004 and Praxis XXI, is gratefully acknowledged. This paper benefited much from the reviewers' comments.

Supporting Information Available: Cartesian coordinates, relevant internal coordinates, and absolute Gibbs energies for all of the stationary species. This material is available free of charge via the Internet at <http://pubs.acs.org>.

References and Notes

- (1) Matsson, O.; Dybala-Defratyka, A.; Rostkowski, M.; Paneth, P.; Westaway, K. C. *J. Org. Chem.* **2005**, *70*, 4022.
- (2) Hasanayn, F.; Streitwieser, A.; Al Rifai, R. *J. Am. Chem. Soc.* **2005**, *127*, 2249.
- (3) Vayner, G.; Houk, K. N.; Jorgensen, W. L.; Brauman, J. I. *J. Am. Chem. Soc.* **2004**, *126*, 9054.
- (4) Ren, Y.; Chu, S. Y. *J. Phys. Chem. A* **2004**, *108*, 7079.
- (5) Ren, Y.; Chu, S. Y. *J. Comput. Chem.* **2004**, *25*, 461.
- (6) Angel, L. A.; Ervin, K. M. *J. Phys. Chem. A* **2004**, *108*, 9827.
- (7) Gronert, S.; Fagin, A. E.; Okamoto, K.; Mogali, S.; Pratt, L. M. *J. Am. Chem. Soc.* **2004**, *126*, 12977.
- (8) Bachrach, S. M.; Chamberlin, A. C. *J. Org. Chem.* **2003**, *68*, 4743.
- (9) Wang, Y. F.; Hase, W. L.; Wang, H. B. *J. Chem. Phys.* **2003**, *118*, 2688.
- (10) Pagliai, M.; Raugei, S.; Cardini, G.; Schettino, V. *J. Chem. Phys.* **2003**, *119*, 9063.
- (11) Mugnai, M.; Cardini, G.; Schettino, V. *J. Phys. Chem. A* **2003**, *107*, 2540.
- (12) Friegen, T. D.; McMahon, T. B. *J. Phys. Chem. A* **2003**, *107*, 668.
- (13) Castejon, H.; Wiberg, K. B.; Sklenak, S.; Hinz, W. *J. Am. Chem. Soc.* **2001**, *123*, 6092.
- (14) Castejon, H.; Wiberg, K. B. *J. Am. Chem. Soc.* **1999**, *121*, 2139.
- (15) Angel, L. A.; Ervin, K. M. *J. Phys. Chem. A* **2001**, *105*, 4042.
- (16) Bentley, T. W.; Roberts, I. *J. Phys. Org. Chem.* **2005**, *18*, 96.
- (17) Ghosh, K. K.; Satnami, M. L.; Sinha, D.; Vaidya, J. *J. Mol. Liq.* **2005**, *116*, 55.
- (18) Pinheiro, L. M. V.; Calado, A. R. T.; Reis, J. C. R. *Org. Biomol. Chem.* **2004**, *2*, 1330.
- (19) Sato, H.; Sakaki, S. *J. Phys. Chem. A* **2004**, *108*, 1629.
- (20) McManus, S. P.; Somani, S.; Harris, J. M.; McGill, R. A. *J. Org. Chem.* **2004**, *69*, 8865.
- (21) Galván, I. F.; Martín, M. E.; Aguilar, M. A. *J. Comput. Chem.* **2004**, *25*, 1227.
- (22) Lee, K. S.; Adhikary, K. K.; Lee, H. W.; Lee, B. S.; Lee, I. *Org. Biomol. Chem.* **2003**, *1*, 1989.
- (23) Owczarek, E.; Kwiatkowski, W.; Lemieszewski, M.; Mazur, A.; Rostkowski, M.; Paneth, P. *J. Org. Chem.* **2003**, *68*, 8232.
- (24) Moutiers, G.; Le Guével, E.; Cannes, C.; Terrier, F.; Buncel, E. *Eur. J. Org. Chem.* **2001**, 3279.
- (25) Um, I. H.; Lee, E. J.; Buncel, E. *J. Org. Chem.* **2001**, *66*, 4859.
- (26) Takeuchi, K.; Ushino, T.; Okazaki, T.; Kitagama, T.; Kinoshita, T.; Ohga, Y.; Tanaka, K.; Toda, F. *Bull. Chem. Soc. Jpn.* **2001**, *74*, 363.
- (27) Hirao, H.; Nagae, Y.; Nagaoka, M. *Chem. Phys. Lett.* **2001**, *348*, 350.
- (28) Yoh, S. D.; Cheong, D. Y.; Lee, C. H.; Kim, S. H.; Park, J. H.; Fujio, M.; Tsuno, Y. *J. Phys. Org. Chem.* **2001**, *14*, 123.
- (29) Humeres, E.; Nunes, R. J.; Machado, V. G.; Gasques, M. D. G.; Machado, C. *J. Org. Chem.* **2001**, *66*, 1163.
- (30) Alfaia, A. J. I.; Calado, A. R. T.; Reis, J. C. R. *Eur. J. Org. Chem.* **2000**, 3627.
- (31) Kondo, Y.; Urade, M.; Yamanishi, Y.; Chen, X. *J. Chem. Soc., Perkin Trans. 2* **2002**, 1449.
- (32) Truong, T. N.; Truong, T. T. T.; Stefanovich, E. V. *J. Chem. Phys.* **1997**, *107*, 1881.
- (33) Lu, Z. Y.; Yang, W. T. *J. Chem. Phys.* **2004**, *121*, 89.
- (34) Soriano, A.; Silla, E.; Tuñón, I.; Martí, S.; Moliner, V.; Bertrán, J. *Theor. Chem. Acc.* **2004**, *112*, 327.
- (35) Nam, K.; Prat-Resina, X.; Garcia-Viloca, M.; Devi-Kesavan, L. S.; Gao, J. L. *J. Am. Chem. Soc.* **2004**, *126*, 1369.
- (36) Loferer, M. J.; Loeffler, H. H.; Liedl, K. R. *J. Comput. Chem.* **2003**, *24*, 1240.
- (37) Lesthaeghe, D.; Van Speybroeck, V.; Marin, G. B.; Waroquier, M. *J. Phys. Chem. B* **2005**, *109*, 7952.
- (38) Graciani, M. D.; Rodríguez, A.; Muñoz, M.; Moyá, M. L. *Langmuir* **2003**, *19*, 8685.
- (39) Muñoz, M.; Graciani, M. D.; Rodríguez, A.; Moyá, M. L. *J. Colloid Interface Sci.* **2003**, *266*, 208.
- (40) Bogdanov, B.; McMahon, T. B. *Int. J. Mass Spectrom.* **2005**, *241*, 205.
- (41) Adamovic, I.; Gordon, M. S. *J. Phys. Chem. A* **2005**, *109*, 1629.
- (42) Solà, M.; Lledós, A.; Duran, M.; Bertrán, J.; Abboud, J.-L. M. *J. Am. Chem. Soc.* **1991**, *113*, 2873.
- (43) Viana, C. A. N.; Calado, A. R. T.; Pinheiro, L. M. V. *J. Chem. Res. (S)* **1992**, 6.
- (44) Viana, C. A. N.; Calado, A. R. T.; Pinheiro, L. M. V. *J. Phys. Org. Chem.* **1995**, *8*, 63.
- (45) Wong, M. W. *Chem. Phys. Lett.* **1996**, *256*, 391.
- (46) (a) Gonzalez, C.; Schlegel, H. B. *J. Chem. Phys.* **1989**, *90*, 2154. (b) Gonzalez, C.; Schlegel, H. B. *J. Phys. Chem.* **1990**, *94*, 5523.
- (47) Becke, A. D. *J. Chem. Phys.* **1993**, *98*, 5648.
- (48) Becke, A. D. *J. Chem. Phys.* **1992**, *96*, 2155.
- (49) Becke, A. D. *J. Chem. Phys.* **1992**, *97*, 9173.
- (50) Lee, C.; Yang, W.; Parr, R. G. *Phys. Rev. B* **1988**, *37*, 785.
- (51) Wadt, W. R.; Hay, P. J. *J. Chem. Phys.* **1985**, *82*, 284.
- (52) (a) Miertus, S.; Scrocco, E.; Tomasi, J. *J. Chem. Phys.* **1981**, *55*, 117. (b) Tomasi, J.; Persico, M. *Chem. Rev.* **1994**, *94*, 2027.
- (53) Cossi, M.; Rega, N.; Scalmani, G.; Barone, V. *J. Comput. Chem.* **2003**, *24*, 669.
- (54) Bader, R. F. W. *Atoms in Molecules. A Quantum Theory*; Oxford University Press: Oxford, U.K., 1990.
- (55) Bader, R. F. W. *Chem. Rev.* **1991**, *91*, 893.
- (56) Frisch, M. J.; Trucks, G. W.; Schlegel, H. B.; Scuseria, G. E.; Robb, M. A.; Cheeseman, J. R.; Montgomery, J. A., Jr.; Vreven, T.; Kudin, K. N.; Burant, J. C.; Millam, J. M.; Iyengar, S. S.; Tomasi, J.; Barone, V.; Mennucci, B.; Cossi, M.; Scalmani, G.; Rega, N.; Petersson, G. A.; Nakatsuji, H.; Hada, M.; Ehara, M.; Toyota, K.; Fukuda, R.; Hasegawa, J.; Ishida, M.; Nakajima, T.; Honda, Y.; Kitao, O.; Nakai, H.; Klene, M.; Li, X.; Knox, J. E.; Hratchian, H. P.; Cross, J. B.; Bakken, V.; Adamo, C.; Jaramillo, J.; Gomperts, R.; Stratmann, R. E.; Yazyev, O.; Austin, A. J.; Cammi, R.; Pomelli, C.; Ochterski, J. W.; Ayala, P. Y.; Morokuma, K.; Voth, G. A.; Salvador, P.; Dannenberg, J. J.; Zakrzewski, V. G.; Dapprich, S.; Daniels, A. D.; Strain, M. C.; Farkas, O.; Malick, D. K.; Rabuck, A. D.; Raghavachari, K.; Foresman, J. B.; Ortiz, J. V.; Cui, Q.; Baboul, A. G.; Clifford, S.; Cioslowski, J.; Stefanov, B. B.; Liu, G.; Liashenko, A.; Piskorz, P.; Komaromi, I.; Martin, R. L.; Fox, D. J.; Keith, T.; Al-Laham, M. A.; Peng, C. Y.; Nanayakkara, A.; Challacombe, M.; Gill, P. M. W.; Johnson, B.; Chen, W.; Wong, M. W.; Gonzalez, C.; Pople, J. A. *Gaussian 03*, revision B.05; Gaussian, Inc.: Wallingford, CT, 2004.
- (57) AIMPAC: *A suite of programs for the Theory of Atoms in Molecules*; R. F. W. Bader and co-workers (Eds.), McMaster University, Hamilton, Ontario, Canada L8S 4L. Available from <http://www.chemistry.mcmaster.ca/aimpac>.
- (58) Everett, D. H.; Wynne-Jones, W. F. K. *Trans. Faraday Soc.* **1939**, *35*, 1380.
- (59) Hamann, S. D.; le Noble, W. J. *J. Chem. Educ.* **1984**, *61*, 658.

- (60) Nevecná, T.; Bekárek, V.; Pytela, O. *Collect. Czech. Chem. Commun.* **1994**, 59, 1384.
- (61) Krug, R. R.; Hunter, W. G.; Grieger, R. A. *J. Phys. Chem.* **1976**, 76, 2335.
- (62) Krug, R. R.; Hunter, W. G.; Grieger, R. A. *J. Phys. Chem.* **1976**, 76, 2341.
- (63) Krug, R. R.; Hunter, W. G.; Grieger, R. A. *Nature (London)* **1976**, 261, 566.
- (64) Abboud, J.-L. M.; Notario, R.; Bertrán, J.; Solà, M. *Prog. Phys. Org. Chem.* **1993**, 19, 1.
- (65) Mó, O.; Yáñez, M. *J. Phys. Chem. A* **1998**, 102, 8174.
- (66) El Firdoussi, A.; Essefar, M.; Bouab, W.; Abboud, J.-L. M.; Mó, O.; Yáñez, M. *J. Phys. Chem. A* **2004**, 108, 10568.
- (67) Tomasi, J. *Theor. Chem. Acc.* **2004**, 112, 184.
- (68) Cimino, P.; Barone, V. *J. Mol. Struct.: THEOCHEM* **2005**, 729, 1.
- (69) Kondo, Y.; Ogasa, M.; Kusabayashi, S. *J. Chem. Soc., Perkin Trans. 2* **1984**, 2093.
- (70) Kondo, Y.; Izawa, S.; Kusabayashi, S. *J. Chem. Soc., Perkin Trans. 2* **1988**, 1925.
- (71) Kondo, Y.; Kambe, H.; Kusabayashi, S. *J. Chem. Soc., Perkin Trans. 2* **1990**, 915.
- (72) Kondo, Y.; Yano, K.; Fang, O.; Saito, H.; Takagi, T. *J. Chem. Soc., Perkin Trans. 2* **1998**, 1827.
- (73) Barthel, J. M. G.; Krienke, H.; Kunz, W. *Physical Chemistry of Electrolyte Solutions: Modern Aspects*; Springer: New York, 1998; p 3.